

## RESEARCH ARTICLE

10.1002/2014JA020052

## Key Points:

- IRI 2007 is evaluated within the polar cap region
- Diurnal and seasonal variations in the IRI 2007 F<sub>2</sub> peak are poorly represented
- IRI 2007 topside thickness demonstrates notable agreement on the annual mean

## Correspondence to:

D. R. Themens,  
david.themens@unb.ca

## Citation:

Themens, D. R., P. T. Jayachandran, M. J. Nicolls, and J. W. MacDougall (2014), A top to bottom evaluation of IRI 2007 within the polar cap, *J. Geophys. Res. Space Physics*, 119, 6689–6703, doi:10.1002/2014JA020052.

Received 7 APR 2014

Accepted 25 JUN 2014

Accepted article online 27 JUN 2014

Published online 5 AUG 2014

## A top to bottom evaluation of IRI 2007 within the polar cap

David R. Themens<sup>1</sup>, P. Thayil Jayachandran<sup>1</sup>, Michael J. Nicolls<sup>2</sup>, and John W. MacDougall<sup>3</sup>

<sup>1</sup>Department of Physics, University of New Brunswick, Fredericton, New Brunswick, Canada, <sup>2</sup>Center for Geospace Studies, SRI International, Menlo Park, California, USA, <sup>3</sup>Department of Physics and Astronomy, University of Western Ontario, London, Ontario, Canada

**Abstract** Monthly median values of ionospheric peak height (hmF<sub>2</sub>) and density (NmF<sub>2</sub>), derived from ionosonde measurements at four Canadian High Arctic Ionospheric Network (CHAIN) stations situated within the polar cap and Auroral Oval, are used to evaluate the performance of the International Reference Ionosphere (IRI) 2007 empirical ionospheric model during the recent solar minimum between 2008 and 2010. This analysis demonstrates notable differences between IRI and ionosonde NmF<sub>2</sub> diurnal and seasonal behavior over the entire period studied, where good agreement is found during summer periods but otherwise errors in excess of 50% were prevalent, particularly during equinox periods. hmF<sub>2</sub> is found to be marginally overestimated during winter and equinox nighttime, while also being underestimated during summer and equinox daytime by in excess of 25%. These errors are shown to be related to significant mismodeling of the M(3000)F<sub>2</sub> propagation factor. The ionospheric bottomside thickness parameter (B0) is also evaluated using ionosonde measurements. It is found that both of the IRI's internal B0 models significantly misrepresent both seasonal and diurnal variations in bottomside thickness when compared to ionosonde observations, where errors at times exceed 40%. A comparison is also presented between IRI and Resolute (74.75N, 265.00E) Advanced Modular Incoherent Scatter Radar (AMISR)-derived topside thickness. It is found in this comparison that the IRI is capable of modeling ionospheric topside thickness exceptionally well during winter and summer periods but fails to represent significant diurnal variability during the equinoxes and seasonal variations.

### 1. Introduction

The International Reference Ionosphere (IRI) is commonly regarded as “the de facto standard for a climatological specification of ionospheric parameters” [Bilitza and Reinisch, 2008]. It is widely used in applications such as the evaluation of the performance of HF modems [Jodalen et al., 2001] and as a baseline ionosphere in data assimilation models [Komjathy et al., 1998; Hernandez-Pajares et al., 2002; Bust et al., 2004; Schmidt et al., 2008; Pezzopane et al., 2011; Galkin et al., 2012]. At midlatitudes, the IRI offers accurate modeled ionospheric parameters, such as the heights and peak electron densities of the ionosphere's various layers, as well as total electron content (TEC), a measure of the total number of electrons in a column through the ionosphere [Coisson et al., 2006; Bilitza et al., 2012]. The same cannot necessarily be said for its application to high-latitude regions, like the polar cap, where there is a significant lack of available data. Also, in contrast to midlatitude regions, where production dominates ionospheric variability, high-latitude ionospheric variability is dominated by transport processes and particle precipitation events over a significant portion of the annual cycle [MacDougall and Jayachandran, 2007].

This study undertakes a thorough evaluation of key IRI parameters including F<sub>2</sub> peak electron density (NmF<sub>2</sub>), F<sub>2</sub> peak height (hmF<sub>2</sub>), M(3000)F<sub>2</sub> propagation factor, bottomside thickness (B0), and topside thickness. There have been several studies that have evaluated the performance of IRI hmF<sub>2</sub> and NmF<sub>2</sub> products in midlatitude and low-latitude regions [Sethi et al., 2008; Ehinlafa et al., 2010; Ezquer et al., 2011; Bilitza et al., 2012; Wichaipanich et al., 2012], but only a select few have attempted to do so in high-latitude regions [Oyeyemi et al., 2010; Ezquer et al., 2011; Magdaleno et al., 2011; Maltseva et al., 2013], none of which have been within the polar cap or at magnetic latitudes as high as what we shall be considering in this study. The performance of the IRI bottomside thickness models has been evaluated mainly in equatorial and midlatitude regions [Sethi and Mahajan, 2002; Blanch et al., 2007; Adeniyi et al., 2008; McKinnell et al., 2009; Lee and Reinisch, 2012], where virtually no evaluation has been undertaken at high latitudes. In terms of topside

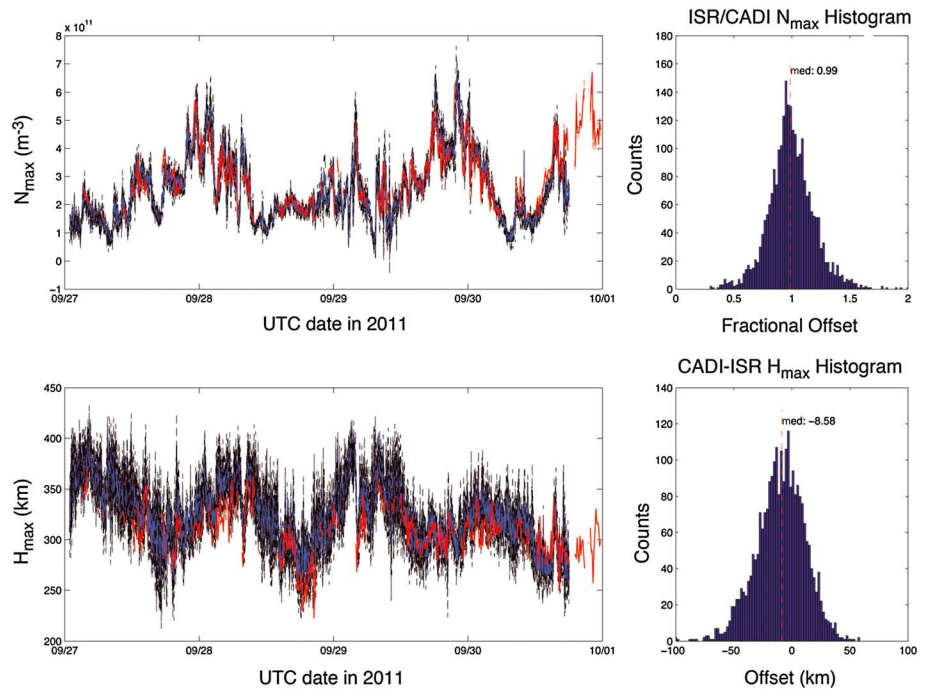


**Figure 1.** Example of ionosonde—Resolute Incoherent Scatter Radar (RISR-N) (top) ionospheric peak density (NmF<sub>2</sub>) and (bottom) ionospheric peak height (hmF<sub>2</sub>) comparison after calibration. RISR-N mean (black) and median (blue) curves for elevation angles greater than 60° are compared to Canadian Advanced Digital Ionosonde (CADI) (red) NmF<sub>2</sub> and hmF<sub>2</sub> measurements. Right panels show histograms of the ratio of RISR-N to CADI NmF<sub>2</sub> (top) and hmF<sub>2</sub> deviation (bottom). Mean and median ratios for the electron density are ~0.99 +/- 0.02 (standard deviation of ~20%).

electron density, it has been shown that the topside model of pre-2007 versions of the IRI demonstrates poor performance at high and equatorial latitudes [Coisson *et al.*, 2002; Bilitza, 2004, 2009]. With the publication of IRI 2007, citing various corrections to high-latitude electron density products, it is crucial that these corrections be appropriately evaluated in the polar cap region [Bilitza and Reinisch, 2008]. In all cases, the IRI has been found to demonstrate notable difficulty in modeling ionospheric characteristics during the extended solar minimum of solar cycle 23/24 [Lühr and Xiong, 2010; Bilitza *et al.*, 2012].

The following section will outline the data sources used in the subsequent analysis. Comparisons between IRI-modeled and ionosonde-derived NmF<sub>2</sub> are presented in section 3.1, followed by an evaluation of IRI hmF<sub>2</sub> products in section 3.2. To diagnose the reason for errors in IRI-modeled hmF<sub>2</sub>, a comparison between ionosonde-derived and IRI-modeled M(3000)F<sub>2</sub> is presented in section 3.3. Finally, the IRI's bottomside thickness parameterizations are evaluated in section 3.4 through the use of ionosonde profiles, while the topside thickness is evaluated in section 3.5 using incoherent scatter radar (ISR) data. Conclusions are presented in section 4.

## 2. Data

In this study, we make use of several radio remote sensing instruments active within the polar cap region including both a network of ionosondes and the Advanced Modular Incoherent Scatter Radar (AMISR) in operation in Resolute, Canada.

### 2.1. Resolute AMISR

The northward-looking face of the Resolute Incoherent Scatter Radar (RISR-N) is a deployment of the AMISR class of ISRs located in Resolute, Canada (74.73°N, -94.91°E). See Bahcivan *et al.* [2010] for system details.

The incoherent scatter technique [e.g., Evans, 1969] provides measurements of the thermal properties of the ionospheric plasma, including electron densities, electron and ion temperatures, and ion drifts. Of paramount importance to the study presented in this paper are calibrated electron density profiles.

**Table 1.** CHAIN Station Geographic Locations and Status

Station	Latitude (°N)	Longitude (°E)	Status
Eureka	79.99	274.03	Operational
Resolute Bay	74.75	265.00	Operational
Pond Inlet	72.69	282.04	Operational
Cambridge Bay	69.12	254.97	Operational
Hall Beach	68.78	278.74	Operational
Iqaluit	63.73	291.46	In testing phase

RISR-N measurements are calibrated using two techniques. During summer daytime periods plasma line measurements, which provide a sensitive measure of Langmuir waves and hence electron densities, are used as an absolute measure of electron density. In other periods manually scaled NmF<sub>2</sub> measurements from an ionosonde system at Resolute are used, when available, to provide a robust, accurate density calibration.

Given that the RISR-N system calibration may change with viewing direction, a further calibration step is required wherein long-term (at least several day) averages are used to normalize the calibration from different viewing directions. It is anticipated that with a proper calibration data set, densities should be accurate to better than 10%; nonetheless, only peak-relative electron densities are used in this study.

An example of a calibration comparison between RISR-N and the Resolute ionosonde system for a 4 day data set at the end of September 2011 is shown in Figure 1. The mean ratio of the ISR-ionosonde density is 0.99 ± 0.02, and the densities track each other well on both short and long time scales. The peak height of the F region, measured by the two instruments, generally agrees within a standard deviation of ~15 km. This excellent agreement is found despite the fact that the instruments use very different techniques and are not probing a common volume.

## 2.2. Ionosonde

### 2.2.1. Canadian Advanced Digital Ionosonde (CADI)

The Canadian High Arctic Ionospheric Network (CHAIN) provides a unique opportunity to undertake an evaluation IRI performance during the minimum of solar cycle 23/24 and rising phase of solar cycle 24 [Jayachandran *et al.*, 2009]. CHAIN operates 10 stations in the Canadian Arctic region that are each equipped with a dual-frequency Global Positioning System (GPS) receiver, six of which are collocated with a Canadian Advanced Digital Ionosonde (CADI). These systems allow for the accurate estimation of TEC and bottomside electron density parameters in the Auroral Oval and polar cap regions [Themens *et al.*, 2013]. Table 1 lists the geographic location of the six CHAIN CADI stations and also identifies the operational capacity of each station. Only the Cambridge Bay, Pond Inlet, Resolute, and Eureka stations are used in this study.

For this study, over 120,000 virtual height ionograms have been manually scaled from CHAIN's database of Cambridge Bay, Pond Inlet, Resolute, and Eureka CADI data. These manually scaled ionograms were inverted to determine real height electron density profiles through the use of the Polynomial Analysis (POLAN) method [Titheridge, 1985, 1988].

CADI-derived M(3000)F<sub>2</sub>, used in the following analysis, is calculated by taking the ratio of the Maximum Usable Frequency at 3000 km (MUF(3000)) to the F region peak critical frequency (foF<sub>2</sub>). The MUF(3000) is directly retrieved from the manually scaled ionograms using the standard transmission curve technique of Smith [1939] with a secant correction factor of 1.116 [Wieder, 1955].

The CADI-derived B<sub>0</sub> thickness parameter, used in the following analysis, was retrieved using a least squares fit of Relation (1) to the CADI bottomside true height electron density profiles down to 0.24 NmF<sub>2</sub>, or to NmF<sub>1</sub> if an F<sub>1</sub>-layer is present,

$$N(h) = NmF_2 \frac{\exp(-x^{B_1})}{\cosh(x)} \quad (1)$$

where  $x = (hmF_2 - h)/B_0$  [Sethi and Mahajan, 2002; Sethi and Pandey, 2001].

Ionograms are available in either 1 or 5 min temporal resolution and 6 km altitude resolution from the CHAIN network, depending on the station and time of study. All data after the summer of 2009 is at 1 min temporal resolution. To reduce the amount of manual scaling required for this study, ionograms were only scaled in 10 min resolution.

### 2.2.2. Qaanaaq/Thule Digisonde

In order to define the IRI's performance in modeling polar cap NmF<sub>2</sub> prior to the extended solar minimum of cycle 23/24, we shall also make use of a Digisonde in operation at Qaanaaq/Thule, Greenland (77.5°N, 290.8°E). Constant-operation data from this station have been gathered from the Global Ionospheric Radio Observatory

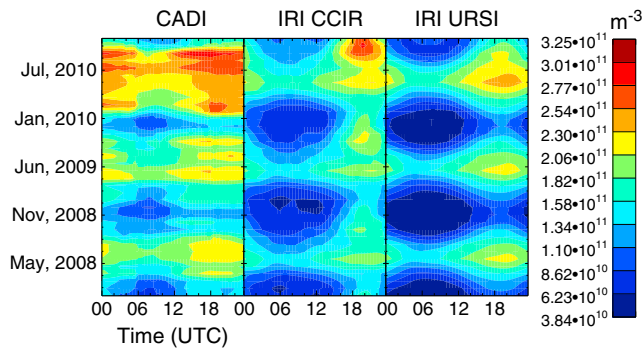


**Figure 2.** CADI-measured and International Reference Ionosphere (IRI)-modeled NmF<sub>2</sub> using both Consultative Committee on International Radio (CCIR) and International Union of Radio Science (URSI) coefficient maps at Resolute between 2008 and 2011.

(GIRO) Digital Ionogram Database (DIDBase) for the period between 2004 and 2011 [Reinisch *et al.*, 2004]. These Qaanaaq ionograms have been autoscaled and inverted using the Automatic Real-Time Ionogram Scaler with True height (ARTIST) autoscaling program [Reinisch *et al.*, 2005]. Due to a series of additional complications inherent in the autoscaling of high-latitude ionograms, namely spread-F, Z-mode propagation, and mode splitting due to travelling ionospheric disturbances (TIDs), we limit the use of these data to the NmF<sub>2</sub> portion of this study [Moskaleva and Zaalov, 2013].

### 2.3. The International Reference Ionosphere (IRI)

The IRI is an empirical, climatological model of the ionosphere based on a host of data sets from around the world, including the global network of ionosondes, incoherent scatter radars, the ISIS and Alouette topside sounders, and various rocket observations. It is developed and maintained by a Committee on Space Research (COSPAR) and International Union of Radio Science (URSI) joint task group, which regularly updates the model's coefficients and proposes improvements for future versions of the IRI [Bilitza and Reinisch, 2008]. The available IRI code can output various ionospheric parameters and allows for the application of a selection of topside, bottomside, and foF<sub>2</sub> coefficient models.

In this paper we undertake an evaluation of the IRI's electron density profile performance, focusing on hmF<sub>2</sub>, NmF<sub>2</sub>, M(3000)F<sub>2</sub>, topside scale parameter, and B0 bottomside thickness parameter. The IRI uses Consultative Committee on International Radio (CCIR) and URSI maps of foF<sub>2</sub>, scaled to solar activity, to construct NmF<sub>2</sub>. For hmF<sub>2</sub>, the IRI uses a modified form of the Bradley-Dudeney formulation, where CCIR M(3000)F<sub>2</sub> maps are used in cooperation with foF<sub>2</sub> and foE in order to determine hmF<sub>2</sub> [Bilitza *et al.*, 1979]. The parameterization used in the IRI is given by the following

$$hmF2 = \frac{1490}{M(3000)F2 + \Delta M} - 176 \tag{2}$$

$$\Delta M = \frac{F_1(R_{12}) \cdot F_2(R_{12}, \Phi)}{foF2/foE - F_3(R_{12})} + F_4(R_{12}) \tag{3}$$

where R<sub>12</sub> is the 12 month smoothed sunspot number, Φ is the modified dip latitude, F<sub>1</sub>, F<sub>2</sub>, F<sub>3</sub>, and F<sub>4</sub> are empirical coefficient functions to account for solar activity [Bilitza *et al.*, 1979].

For B0, the IRI provides two options: table values developed using ionosonde measurements that were revised in IRI 2000 [Bilitza, 2001, 2003; Bilitza *et al.*, 2000], and the Gulyaeva Model of Gulyaeva [1987], which was developed using midlatitude observations and is only recommended for use in midlatitude regions. Both of these model options are evaluated in this study.

IRI 2007 features a revised topside ionospheric model; in particular, it allows for the use of a revised version of the IRI 2001 topside or the use of the NeQuick topside [Bilitza, 2009]. The revised IRI 2001 topside, which is not evaluated in this study, is an exponential layer with a modified Booker scale function [Bilitza, 1990; Bilitza, 2004; Coisson *et al.*, 2006] while the NeQuick topside is a modified Epstein layer with an empirically defined scale factor [Coisson *et al.*, 2006, 2009].

For this study, we have developed an Interactive Data Language (IDL) command line code in order to interface with the IRI 2007 code available from the National Space Science Data Center FTP site at <http://spdf.gsfc.nasa.gov/pub/models/iri/>. This code retains all of the functionality of the original IRI 2007 scripts, including the capability for user specification of measured hmF<sub>2</sub> and NmF<sub>2</sub> values, which is used in sections 3.2 and 3.5 to help diagnose the cause of observed errors in IRI hmF<sub>2</sub> and topside scale parameter.

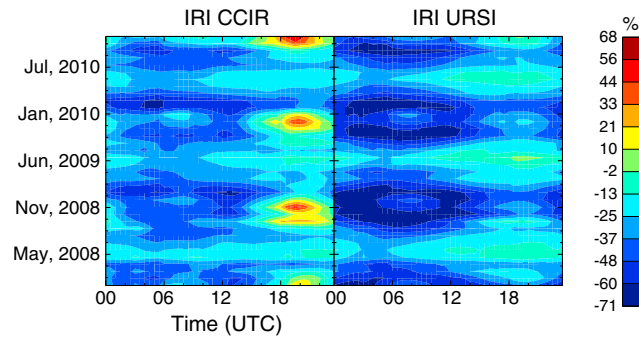


**Figure 3.** Percent differences between CADI and IRI NmF<sub>2</sub> using both CCIR and URSI coefficient maps at Resolute.

### 3. Results and Discussion

In order to evaluate IRI performance within the polar cap region, we shall compare four key parameters that govern the structure of the majority of the IRI's electron density profile, namely NmF<sub>2</sub>, hmF<sub>2</sub>, bottomside thickness (B0), and topside thickness, through the use of percent and monthly RMS differences.

#### 3.1. NmF<sub>2</sub>

NmF<sub>2</sub>, or foF<sub>2</sub>, is an extremely important parameter in the IRI model, as the majority of the IRI electron density profile is scaled to the density at the F region peak. In addition to this, foF<sub>2</sub> is a primary parameter in the estimation of the IRI's NeQuick topside thickness and is also used in IRI hmF<sub>2</sub> estimation. Proper modeling of NmF<sub>2</sub> within the IRI model is thus integral to the model's capability to be used as a baseline model in HF communications or positioning forecasting [Komjathy et al., 1998; Hernandez-Pajares et al., 2002]. In order to evaluate the IRI's performance within the polar cap, we begin by comparing monthly median CADI-measured and IRI-modeled NmF<sub>2</sub>. An example of this comparison at the CHAIN station in Resolute is presented in Figure 2, where we have plotted contour plots of CADI and IRI NmF<sub>2</sub> values, using both the URSI and CCIR coefficient options, for the period of 2008–2011. Qualitatively from this figure, the URSI option fails to demonstrate equinox enhancements in daytime NmF<sub>2</sub>, apparent in the ionosonde data, during the period studied. Examining the CCIR option, a seasonal phase shift is observed, particularly during the increasing phase of solar cycle 24, where the seasonal maximum in daytime CCIR NmF<sub>2</sub> appears to be delayed by over a month. On the whole, both models appear to consistently underestimate nighttime NmF<sub>2</sub> for all but summer periods. Over diurnal cycles, both the CCIR and URSI models appear to terminate the daytime enhancement in NmF<sub>2</sub> too soon in the day. This lack of a persistent daytime NmF<sub>2</sub> enhancement is likely the result of transport processes playing a much more significant role in F region dynamics at high latitudes, as compared to the low latitude and midlatitude where the majority of the model calibration was undertaken.

In Figure 3 we present the percent differences between CADI and IRI NmF<sub>2</sub> for the same period and station. URSI NmF<sub>2</sub> demonstrates good agreement in summer months, particularly during the daytime, where agreement is generally within ~10%. During the summer nighttime, errors are found to remain within 25%. Performance during equinox periods is, however, not encouraging, as errors during equinox nighttime are found to exceed 65%, at times, and daytime errors never fall below 25%. This pattern of increased error during periods of little solar-driven production likely arises due to transport process, which could not be observed in the primarily midlatitude data sets used to generate the model.

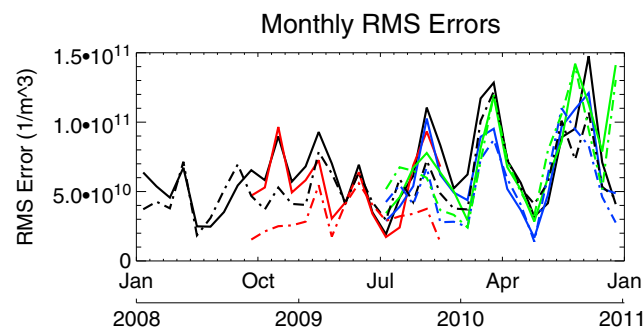


**Figure 4.** Monthly RMS errors between CADI and IRI NmF<sub>2</sub> using CCIR (dashed) and URSI (solid) coefficient maps at Resolute (black), Eureka (red), Pond Inlet (blue), and Cambridge Bay (green).

Looking at the CCIR option, we again observe a pattern of improved agreement during periods of solar-production dominated dynamics. NmF<sub>2</sub> during summer daytime is found to be underestimated by no more than 20%, increasing to roughly 30% during summer nighttime periods. During the equinoxes, trends are found to be similar to those of the URSI option, where NmF<sub>2</sub> is underestimated by up to 60% during nighttime periods and 30% during daytime periods. In contrast to URSI observations, the CCIR option significantly over estimates the

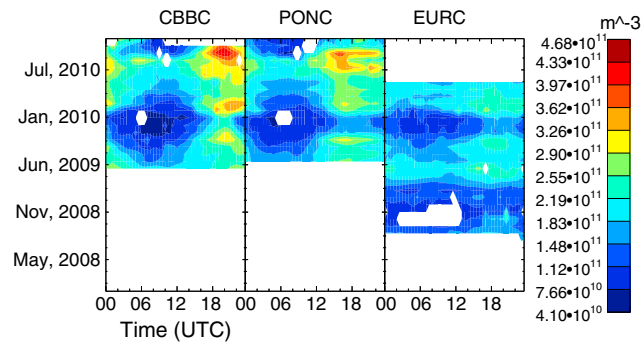


**Figure 5.** CADI-derived NmF<sub>2</sub> from the Cambridge Bay, Pond Inlet, and Eureka Canadian High Arctic Ionospheric Network (CHAIN) stations.

but performs particularly well during summer periods, outperforming the CCIR option. In all other periods, the CCIR option outperforms the URSI option, doing particularly well in winter periods. Both options demonstrate notable error in equinox months, as neither of the options demonstrates the spring daytime enhancement in NmF<sub>2</sub> that is obvious in the CADI data. Also of note is an almost linear increase in equinox NmF<sub>2</sub> RMS errors with increasing solar activity over the period studied, particularly while using the URSI option. This could be the result of there being a characteristically different relationship between solar activity and peak electron density at high latitudes, as compared to low latitude and midlatitude. This will be investigated in future work.

We may also observe the largely similar error patterns at all stations, demonstrating statistically insignificant differences between each. In Figure 5 we present contour plots of the NmF<sub>2</sub> from the remaining three CHAIN stations. As can be seen, all four CHAIN stations demonstrate consistent solar cycle, seasonal, and diurnal behavior in NmF<sub>2</sub>, where NmF<sub>2</sub> decreases with increasing latitude during the photoionization dominated summer daytime and NmF<sub>2</sub> increases with increasing latitude during the transport dominated winter nighttime.

In order to characterize the effect of the extended solar minimum on IRI performance within the polar cap, we present Qaanaaq/Thule Digisonde and IRI NmF<sub>2</sub> data for the period between 2004 and 2011 in Figure 6, as well as percent differences in Figure 7. From these figures, we may note that the percent differences between

magnitude of winter diurnal variability, overestimating winter daytime NmF<sub>2</sub> by up to 65% while underestimating nighttime values by up to 35%.

In order to compare the performance of both IRI NmF<sub>2</sub> options, monthly RMS errors for both the URSI and CCIR options, for all CHAIN CADI stations, are presented in Figure 4. From this figure, it is clear that the CCIR model performs best during early winter and during summer periods. The URSI model performs best during the same periods

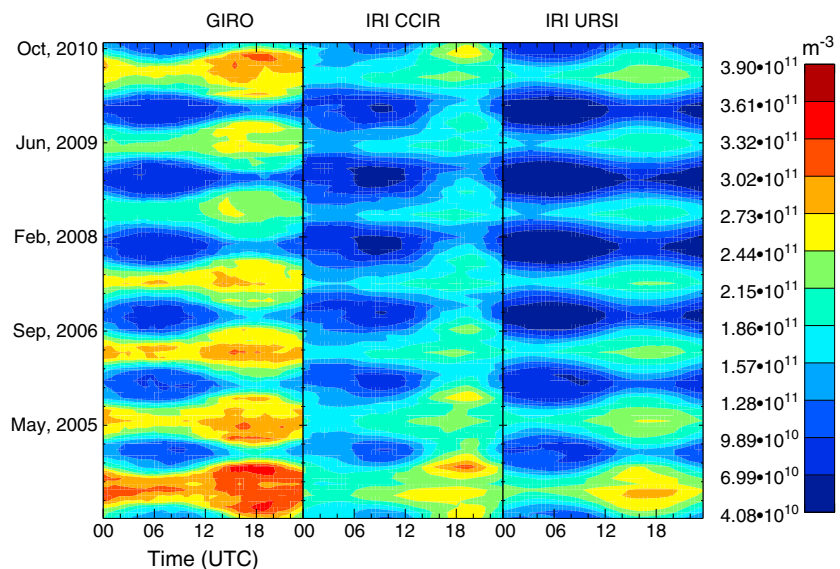


**Figure 6.** Digisonde and IRI-modeled NmF<sub>2</sub> using URSI and CCIR coefficient maps at the Qaanaaq Global Ionospheric Radio Observatory (GIRO) station between 2004 and 2011.

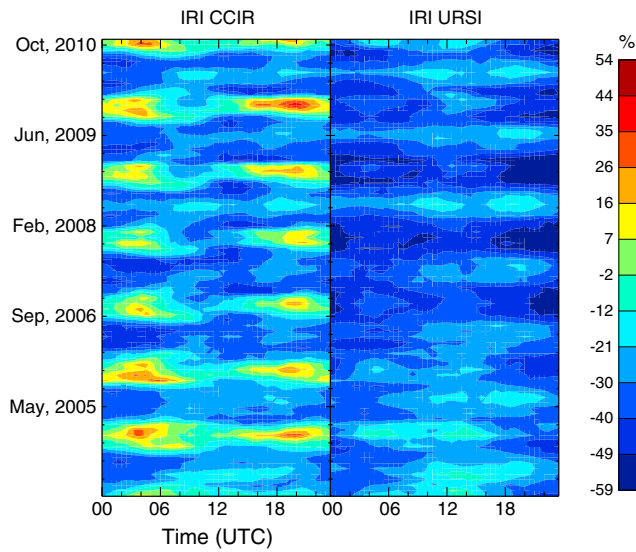


**Figure 7.** Percent differences between Digisonde and IRI NmF<sub>2</sub> using URSI and CCIR coefficient maps at Qaanaaq.

IRI and Digisonde NmF<sub>2</sub> increase significantly during the solar minimum period. In particular, between 2004 and 2008 the magnitude of percent differences between URSI and Digisonde NmF<sub>2</sub> during the winter and equinox nighttime increases from 35% to more than 50%, while errors during summer months remain roughly constant. Errors between Digisonde and CCIR NmF<sub>2</sub>, however, remain roughly consistent, steadily demonstrating fair (within 20%) agreement during early winter and fall equinox periods and underestimation of 40–50% during all other seasons. These results are consistent with the errors observed at the CHAIN stations.

Absolute RMS differences between IRI and Digisonde NmF<sub>2</sub> are presented in Figure 8. While, in terms of percent differences, the IRI appears to perform much better during periods of high solar activity, RMS errors between IRI and Digisonde NmF<sub>2</sub> in fact decrease significantly during the extended solar minimum. This is particularly observed during summer periods, where NmF<sub>2</sub> performance increases significantly over the course of the extended solar minimum, particularly while using the URSI option.

Both the CADI and Digisonde results demonstrate comparable error patterns in the IRI's NmF<sub>2</sub> products.

**3.2. hmF<sub>2</sub>**

The modeling of hmF<sub>2</sub> can have significant implications on the accuracy of IRI-modeled TEC and thus must be evaluated prior to the IRI's use as a potential model for positioning applications. In this study we use hmF<sub>2</sub> inverted from CADI virtual height ionograms to determine the accuracy of IRI-modeled hmF<sub>2</sub> within the high-latitude polar cap region. Relations 2 and 3 imply that the choice of foF<sub>2</sub> map (CCIR or URSI) within the IRI model could have a significant impact on IRI hmF<sub>2</sub> values, and thus, errors in foF<sub>2</sub> could further propagate as errors in hmF<sub>2</sub>. In Figure 9 we present the hmF<sub>2</sub> measured by CADI and that modeled by the IRI using the CCIR and URSI foF<sub>2</sub> maps, as well as IRI-modeled hmF<sub>2</sub> using CADI foF<sub>2</sub> values ingested into the model. It is easy to see from this figure that the choice of foF<sub>2</sub> can have a significant impact on the IRI-modeled hmF<sub>2</sub>, at times resulting in differences between hmF<sub>2</sub>, using CCIR or CADI foF<sub>2</sub> exceeding 60 km.

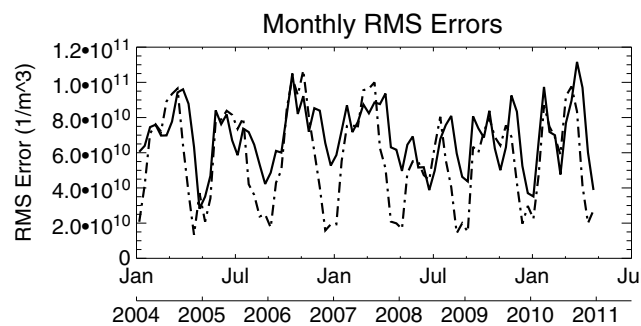


**Figure 8.** Monthly RMS errors between Digisonde and IRI NmF<sub>2</sub> using URSI (solid) and CCIR (dashed) coefficient maps at Qaanaaq between 2004 and 2011.

In Figure 10 we present the percent differences between CADI-derived and IRI-modeled hmF<sub>2</sub> using all three foF<sub>2</sub> options. IRI hmF<sub>2</sub> derived using the CCIR foF<sub>2</sub> option underestimates equinox daytime hmF<sub>2</sub> by upward of 25% during the deepest phase of the extended solar minimum. During summer periods, hmF<sub>2</sub> is slightly underestimated by roughly 5% to 10%. During nighttime periods, with the exception of the summer, hmF<sub>2</sub> is slightly overestimated by between 3% and 9%. Using the URSI foF<sub>2</sub> map, we find that those errors observed in the spring and summer daytime during the solar

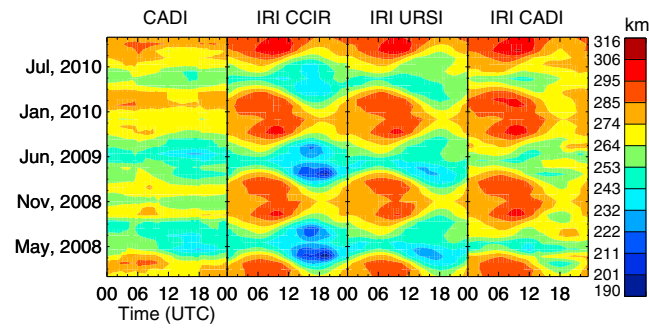


**Figure 9.** CADI-derived and IRI-modeled hmF<sub>2</sub> using URSI, CCIR, and CADI foF<sub>2</sub> at Resolute between 2008 and 2011.

minimum are less pronounced, decreasing to within 15%. Overall, the URSI option demonstrates appreciable improvement over the use of the CCIR foF<sub>2</sub> option. All three options overestimate winter and equinox nighttime hmF<sub>2</sub> by approximately 10%, producing a less obvious semi-annual variation. These observations are consistent with the observations of Oyeyemi *et al.* [2010] and Magdaleno *et al.* [2011] at their Sondrestrom (66.98°N, 309.06°E) and College (69.9°N, 212.2°E) stations.

We may also note that the ingestion of CADI foF<sub>2</sub> into the IRI produces little improvement in hmF<sub>2</sub> results and even increases errors at times. What little improvement that is observed is largely constrained to spring equinox periods. This result can be easily explained by examining the effect of foF<sub>2</sub> in Relations (2) and (3). From this relationship, it is easy to show that an increase in foF<sub>2</sub> will result in a corresponding increase in modeled hmF<sub>2</sub>. During the spring equinox, the CCIR and URSI options tend to overestimate the diurnal variability of foF<sub>2</sub>. Since the IRI tends to overestimate hmF<sub>2</sub> variability during this period as well, the decreased diurnal variability of CADI foF<sub>2</sub> values corrects some of this overestimation. Agreement during these periods between CADI hmF<sub>2</sub> and that modeled by the IRI with CADI foF<sub>2</sub> ingested into the model suggests that M(3000)F<sub>2</sub> maps likely perform best during these periods. In most nighttime periods, however, the CCIR and URSI options tend to underestimate foF<sub>2</sub> but overestimate hmF<sub>2</sub>; thus, ingesting the higher foF<sub>2</sub> from the CADI data has the effect of further overestimating hmF<sub>2</sub>. During the daytime, both options tend to underestimate the persistence and intensity of daytime foF<sub>2</sub> enhancements; thus, significant differences arise during these periods.

These results can also be examined through the use of RMS errors, which are presented in Figure 11. One may observe that the IRI performs best during the summer while performing its worst at the equinoxes for all both IRI foF<sub>2</sub> options. These errors at the equinoxes are a direct result of the IRI's overestimation of the magnitude of diurnal variability during these periods. Looking at the CADI-ingested RMS results, errors are observed to be at a minimum during the spring and at their worst during the summer. Errors using all three foF<sub>2</sub> options appear to decrease as solar activity increases in 2010.

Assuming that Relations (2) and (3) are correct, these results, particularly those featuring CADI foF<sub>2</sub> ingestion, imply that there are significant errors within the IRI M(3000)F<sub>2</sub> map, which are most significant during the extended solar minimum period. Namely, based on the overestimation of hmF<sub>2</sub> observed in the CADI-ingested IRI results, it is likely that the IRI significantly underestimates MUF(3000)F<sub>2</sub> during the summer daytime and the nighttime of the remaining seasons, where errors are largest during the extended solar minimum.

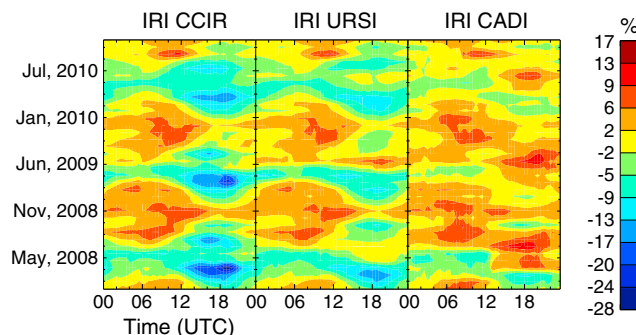


**Figure 10.** Percent differences between CADI and IRI hmF<sub>2</sub> at Resolute for each of the options of Figure 10.

### 3.3. M(3000)F<sub>2</sub>

To verify the hypothesis identified in section 3.2, we have undertaken an evaluation of IRI M(3000)F<sub>2</sub> using CADI-derived values. Monthly median values of M(3000)F<sub>2</sub> from both CADI and the IRI at Resolute between 2008 and 2011 have been plotted in Figure 12. The problem of underestimated hmF<sub>2</sub>, identified in the previous section of this study, is clearly evident in this figure. As one can see there is a striking error in the

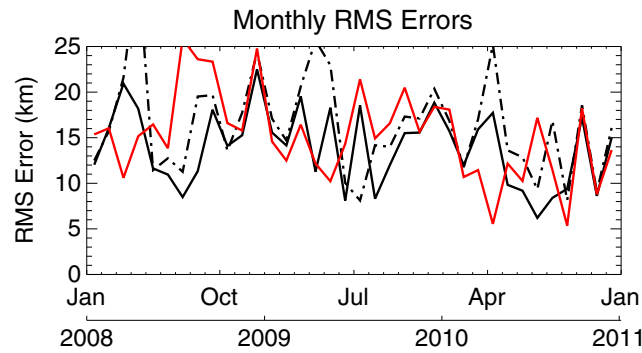


**Figure 11.** Monthly RMS errors between CADI and IRI hmF<sub>2</sub> using URSI (solid black), CCIR (dashed black), and CADI (solid red) foF<sub>2</sub> at Resolute.

IRI's M(3000)F<sub>2</sub> maps, particularly in summer periods, where the model demonstrates the opposite diurnal behavior of the CADI observations. Percent differences for this data are presented in Figure 13, where we can now quantify a substantial underestimation in summer and spring daytime M(3000)F<sub>2</sub>. From this figure we observe underestimation of up to 22% during summer and spring daytime F<sub>2</sub> values generally agree to within 5%. Agreement during winter and fall

nighttime periods is in conflict with the hypothesis proposed in section 3.2, as we would expect underestimation similar to that of the summer daytime during these periods based on the hmF<sub>2</sub> results of section 3.2; thus, this suggests a potential issue in the foE parameterization during these periods. In terms of solar activity, the errors observed through this comparison appear to increase with the deepening of the extended solar minimum, consistent with the hypothesis of section 3.2. This is characterized by a strong increase in observed summer daytime maximum M(3000)F<sub>2</sub> during the extended solar minimum while the IRI demonstrates far more marginal solar activity-based variability.

These results are largely consistent with the hmF<sub>2</sub> results observed in section 3.2 (with the exception of the winter nighttime) and have significant implications for the HF communications forecasting community. As the IRI uses the CCIR M(3000)F<sub>2</sub> maps to directly model this parameter, these results reflect a significant mis-modeling of high-latitude M(3000)F<sub>2</sub> by the CCIR model. This CCIR model is used, with some adjustments, in a variety of important HF communications forecasting models. The implications of these errors with respect to these HF forecasting models will be investigated in a subsequent study.

**3.4. B0**

B0, although not as important with respect to communications or positioning applications as the topside thickness parameter, has been suggested to be included in the IRI's topside scale factor algorithm [Coïsson et al., 2009], which would make accurate B0 estimation crucial to correctly modeling the topside ionosphere

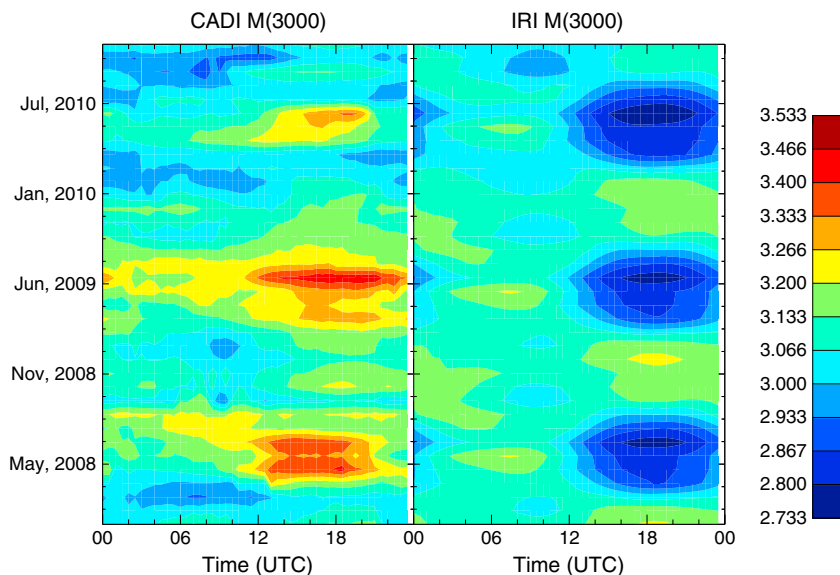


**Figure 12.** CADI-derived and IRI-modeled M(3000)F<sub>2</sub> using at Resolute between 2008 and 2010.

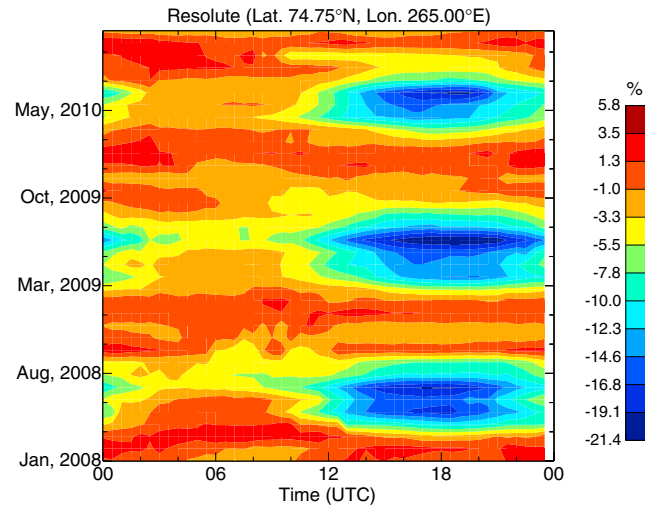


**Figure 13.** Percent differences between CADI and IRI M(3000)F<sub>2</sub> at Resolute between 2008 and 2011.

within the IRI. In Figure 14 we present B<sub>0</sub> estimated using CADI measurements through Relation (1), as well as that modeled by the IRI Table and Gulyaeva options over the CHAIN Resolute station. As can be clearly seen, there are striking differences in the dynamics of the B<sub>0</sub> parameter demonstrated by each model option. In this figure we observe a clear diurnal structure in B<sub>0</sub>, which is largely not modeled by the IRI Table option. During summer and equinox periods B<sub>0</sub> is largest during the daytime and lowest during the nighttime, where the magnitude of diurnal variability is greatest during the equinoxes. During the winter, the phase of the B<sub>0</sub> diurnal variability changes significantly, where

B<sub>0</sub> is found to be largest during the nighttime and lowest during the daytime. This feature is weakly present in both IRI options, where the magnitude of this variability is well represented by the Table option but significantly overestimated by the Gulyaeva option. Summer and equinox daytime B<sub>0</sub> demonstrates a strong coupling with solar activity, where values are lowest during the extended solar minimum and increase significantly during the rising phase of solar cycle 24. Also observed are strong equinox daytime enhancements, which are not represented in either of the IRI options.

In Figure 15 we present the percent differences between CADI-derived and IRI modeled B<sub>0</sub> at the Resolute station between 2008 and 2011. Because the Gulyaeva option poorly models the observed winter reversal in the diurnal variations of B<sub>0</sub>, we find that this option underestimates nighttime winter B<sub>0</sub> more than 30% during the solar minimum period. Both IRI B<sub>0</sub> options overestimate equinox nighttime B<sub>0</sub> by 20% to 35%. The absence of diurnal variability in the Table option leads to underestimation of B<sub>0</sub> by up to 30% during the summer and spring daytime periods and overestimation by between 20% and 30% during winter and fall nighttime periods. In general, both options appear to have difficulty modeling B<sub>0</sub> during 2009, where B<sub>0</sub> is overestimated by up to 50% and 30%, using the Gulyaeva and Table options, respectively. This is, perhaps, due to the abnormally low solar activity during 2009. Also, the absence of a strong coupling between equinox daytime B<sub>0</sub> and solar activity in the IRI model leads to underestimation by up to 25% and 30% by the Gulyaeva and Table products, respectively.

The recent publication of IRI 2012 cites an improved B<sub>0</sub> representation following the harmonic function methodology of Altadill et al. [2009] [Bilitza et al., 2010]. Although such an approach would likely resolve the primary issues observed in this study, namely the over-simplification of B<sub>0</sub> temporal variations in the current IRI Table option, the model does not include a significant database from high-latitude regions; thereby, it

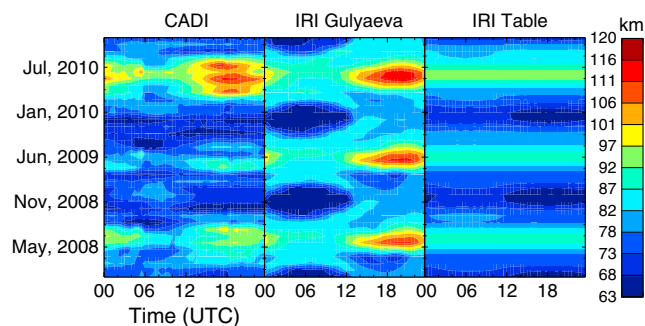


**Figure 14.** CADI-derived and IRI-modeled B<sub>0</sub> at Resolute using both the Gulyaeva and Table options.

remains to be seen whether such IRI improvements can correctly model ionospheric parameters in these regions without the expansion of the baseline data set to include more high-latitude observations. This concern is highlighted in the Gulyaeva results presented above, where diurnal and seasonal structures are present but do not represent the dynamics of the high-latitude region, likely due to the largely midlatitude database used in its creation.

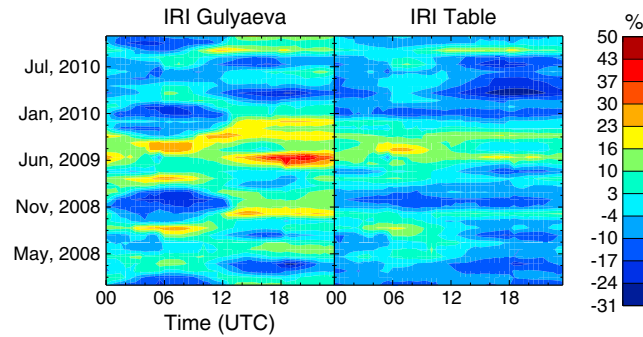


**Figure 15.** Percent differences between CADI and IRI B0 at Resolute using the Gulyaeva and Table options.

**3.5. Lower Topside Region**

The topside ionosphere can sometimes account for more than 75% of ionospheric TEC, making the accurate modeling of this region crucial to using the IRI in positioning applications [Belehaki and Tsagouri, 2002]. In this study, we make use of ISR electron density profiles at Resolute in order to evaluate the IRI's performance in modeling electron density in the lower topside (below 650 km). In Figure 16 we present the seasonal means of F2 peak-

normalized topside electron density contours retrieved from the Resolute ISR for the period between September 2009 and August 2010. F2 peak-normalized refers to normalizing the profiles to the F2 peak density and converting them to peak relative altitude prior to evaluating the seasonal means. Examining this figure, one will observe strong diurnal variability in topside electron density throughout the year studied, with the exception of the winter period. Diurnal variability is greatest during the spring period. Figure 17 presents the seasonal mean trends produced using the IRI with the URSI foF<sub>2</sub> map option. In contrast to the ISR observations, the IRI topside demonstrates little to no diurnal or seasonal variability. The percent differences between IRI-modeled and ISR-measured topside profiles are presented in Figure 18. It is clear from this figure that the IRI demonstrates a seasonal agreement with ISR data, where there is good agreement in the summer and winter months, but poor agreement during the equinoxes. This is characterized by overestimation in the fall and underestimation in the spring. The increasing magnitude of these disagreements with increasing altitude suggests that these errors are due in large part to an error in IRI-modeled topside thickness.

To illustrate this seasonal error trend, we have fit these mean topside ISR and IRI profiles to the NeQuick semi-Epstein layer model given by

$$N(h) = \frac{4 \cdot NmF2}{(1 + \exp(z))^2} \exp(z) \tag{4}$$

$$z = \frac{h - hmF2}{H_o \left[ 1 + \frac{rg(h - hmF2)}{rH_o + g(h - hmF2)} \right]} \tag{5}$$

where  $r = 100$ ,  $g = 0.125$ ,  $h$  is the altitude, and  $H_o$  is the characteristic topside scale factor [Coisson et al., 2006]. In this way, we retrieve a characteristic shape parameter,  $H_o$ , for both data sets. The results of this analysis are presented in Figure 19, where seasonal mean trends in  $H_o$  are presented for the same period as Figures 16, 17, and 18. This figure demonstrates that the IRI is underestimating the seasonal trend in topside shape parameter while also significantly underestimating its diurnal variations in the equinox periods.

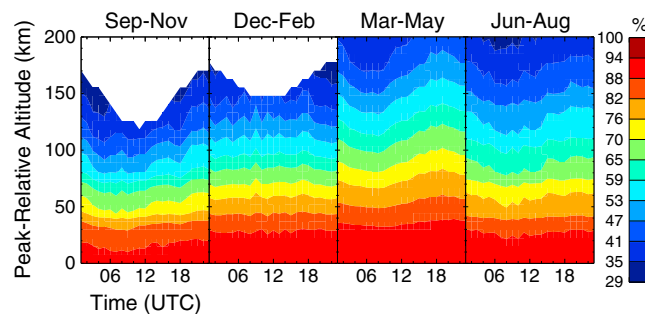


**Figure 16.** ISR-derived, monthly median, peak normalized, topside electron density (as percentage of NmF<sub>2</sub>) at Resolute between September 2009 and August 2010.

This disagreement ranges from 6 km at nighttime to 20 km during daytime in the spring period and ranges from 5 km during the daytime to 15 km at nighttime in the fall period. There is, however, a high degree of agreement between IRI-modeled and ISR-derived topside scale factor during the summer and winter months, where thicknesses are within 5 km at all times. Also, there appears to be strong agreement between ISR and IRI annual means.

The shape parameter used in the IRI's implementation of the NeQuick

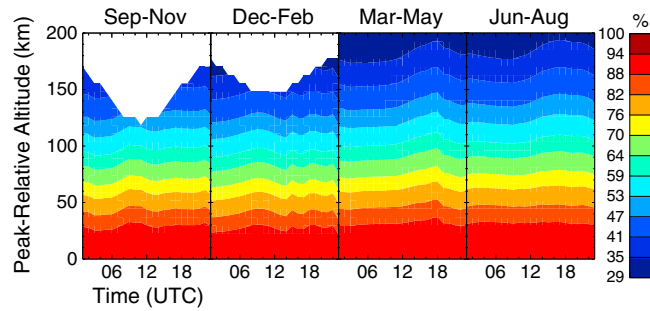


**Figure 17.** IRI-modeled, monthly median, peak normalized, topside electron density (as percentage of NmF<sub>2</sub>) at Resolute between September 2009 and August 2010.

topside is dominated by the calculation of the empirical function  $k$  and of  $B2_{Botr}$ , the characteristic shape parameter associated with a semi-Epstein F2 bottomside. These parameters are calculated using the following parameterizations [Coisson *et al.*, 2009]:

$$H_o = k \cdot B2_{bot} \tag{6}$$

$$k = 3.22 - 0.0538foF2 - 0.00664hmF2 + 0.113 \frac{hmF2}{B2_{bot}} \tag{7}$$

$$B2_{bot} = \frac{0.385NmF2}{(dN/dh)_{max}} \tag{8}$$

$$\ln\left(\frac{dN}{dh}\right)_{max} = -3.467 + 0.857 \ln(foF2)^2 + 2 \ln(M(3000)F2) \tag{9}$$

As one can see, there is a strong dependence on foF<sub>2</sub>, M(3000)F<sub>2</sub>, and hmF<sub>2</sub> in these parameterizations. One may thereby assume that errors in one or more of these parameters, as was illustrated in sections 3.1 and 3.2, should have a profound impact on the IRI topside profile. In order to deduce where the errors in the IRI topside are coming from, we ingest CADI foF<sub>2</sub> and hmF<sub>2</sub> into the IRI and compare the resulting H<sub>o</sub> values with the corresponding ISR-derived values. It should be noted at this point that the IRI uses the CCIR M(3000)F<sub>2</sub> maps in the calculation of the  $\ln(dN/dh)_{max}$  term no matter the parameters ingested into the model. The results of this ingestion are presented in Figure 19, where we may note that there is no appreciable improvement in the IRI topside after ingestion. These results suggest that errors in IRI topside profiles above Resolute are likely the result of errors in the parameterization of the topside scale factor and likely arise due to a lack of topside sounder data in these regions, particularly the lack of data covering complete diurnal and seasonal cycles. This is obvious as the annual means from both ISR and the IRI compare exceptionally well while the IRI fails to adequately represent diurnal and seasonal patterns.

While the new IRI-Plas topside model of Gulyaeva [2003] cites improvements to the IRI topside, investigated here, these improvements are largely limited to the upper portion of the topside

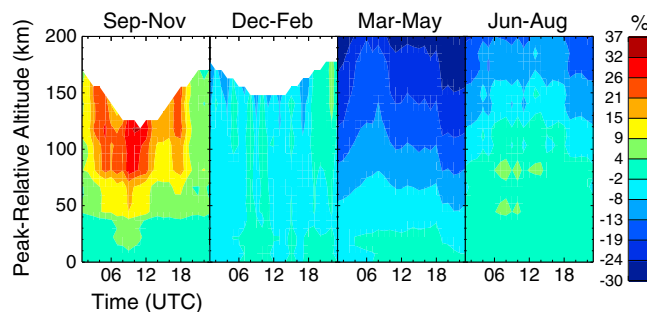


**Figure 18.** Percent differences between IRI and ISR monthly median, peak normalized, topside electron density at Resolute between September 2009 and August 2010.

profile; thus, it is unlikely that the IRI-Plas would demonstrate any notable improvement in the lower topside over the NeQuick model unless a larger high-latitude data set was used in its construction to solve the temporal variability issues identified above. This, however, is just conjecture. A thorough evaluation of IRI-Plas should be undertaken in order to assess any improvement it may provide over the NeQuick in application to the polar cap region.

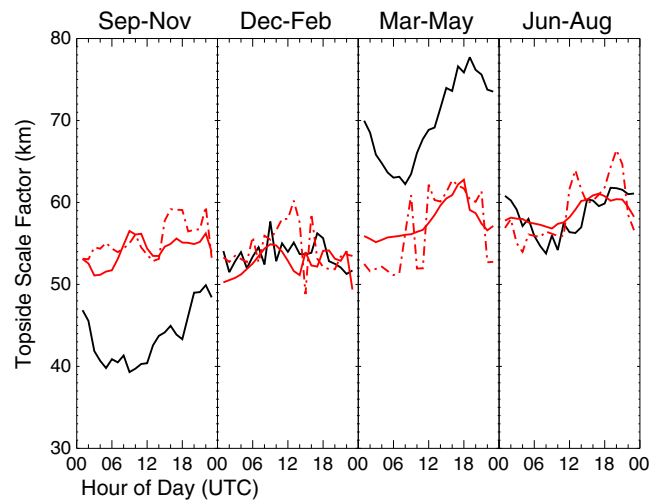


**Figure 19.** Topside scale parameter ( $H_0$ ) derived from ISR (solid black) and IRI topside profiles using URSl fo $F_2$  (solid red) and CADI-ingested fo $F_2$  and hm $F_2$  (dashed red) at Resolute between September 2009 and August 2010.

#### 4. Conclusions

In this study, the IRI's performance in modeling Nm $F_2$ , hm $F_2$ , M(3000) $F_2$ , bottomside thickness, and topside thickness is evaluated within the Canadian Arctic region over the course of the extended solar minimum of cycle 23/24. For Nm $F_2$ , using the URSl option, the IRI fails to represent equinox daytime enhancements in Nm $F_2$ . Using the CCIR option a phase shift in the seasonal behavior of daytime maximum Nm $F_2$  of over a month is observed. For both options, there is a general trend of terminating the daytime Nm $F_2$  enhancement too soon in the day. Also, with the exception of summer periods, both options significantly underestimate nighttime Nm $F_2$ ,

particularly at the equinoxes. These trends are likely the result of unmodeled transport processes that were not observed in the original IRI fo $F_2$  mapping data set. In terms of solar cycle variability, both IRI options demonstrate a local minimum in RMS error during the extended solar minimum of cycle 23/24.

We have also investigated the overall errors in IRI-modeled hm $F_2$  over the extended solar minimum and the effect that fo $F_2$  ingestion can have of IRI performance in modeling this feature. With the exception of equinox daytime periods, the IRI demonstrated only slight errors in hm $F_2$ , where it is overestimated by 3% to 9% during winter and equinox nighttime periods and underestimated by 5% to 10% in summer months. During equinox periods, however, the magnitude of diurnal variability is significantly overestimated by the IRI model leading to equinox daytime underestimation of hm $F_2$  by up to 25%. Ingesting CADI fo $F_2$  into the model appears to produce little improvement in IRI-modeled hm $F_2$  and in fact increases errors during summer daytime periods. These observations suggest that significant errors exist within the CCIR M(3000) $F_2$  maps. This is verified in an evaluation of M(3000) $F_2$  performance, where the IRI demonstrates opposite diurnal behavior from observations in summer and equinox periods.

In terms of bottomside thickness, both IRI options demonstrate significant errors. The IRI Table option demonstrates little to no diurnal variability in B0 during all but winter periods while CADI data suggests variability of up to 35 km during spring and summer periods. The Gulyaeva option demonstrates appreciable diurnal variability but significantly overestimates this variability during winter periods. Both options fail to correctly model equinox enhancements in daytime bottomside thickness resulting in errors of between 25% and 30%. Encouragingly, both IRI options model the winter reversal in B0 variability to some degree.

For the topside, we have compared peak-relative and normalized electron densities from the IRI NeQuick model to those from the AMISR system in operation in Resolute, Canada over the course of a year between September 2009 and August 2010. ISR electron densities demonstrate strong diurnal variability during summer and equinox periods, as well as an obvious seasonal cycle. IRI topside results, however, demonstrate little to no variability on both diurnal and seasonal time scales. This discrepancy is largely attributed to errors in the topside thickness, where errors range from 6 km at nighttime to 20 km during daytime in the spring period and range from 5 km during the daytime to 15 km at nighttime in the fall period. Nonetheless, a high degree of agreement between IRI-modeled and ISR-derived topside scale factor is observed during the summer and winter months, where thicknesses are within 5 km at all times. Despite the observed errors the ISR and IRI thickness agree remarkably well over annual means; thus, errors are likely due to a lack of topside sounder data in these regions, particularly a lack of data covering complete diurnal and seasonal cycles.

The following recommendations are made for those needing to use the IRI 2007 model within the polar cap region: for Nm $F_2$ , one should use the CCIR coefficient maps and limit use to summer periods, where the IRI

model performs exceptionally well; for hmF<sub>2</sub>, one should use the URSI foF<sub>2</sub> coefficient maps; for M(3000)F<sub>2</sub> propagation factor, the authors strongly advise limiting use to winter or nighttime periods; and for topside thickness, one should limit use to summer and winter periods. No recommendations are afforded with regard to bottomside thickness; as such, recommendations must be considered on a case-by-case basis for this parameter.

Future work will examine the overall effect of these observed errors on the IRI's capability to provide TEC in these regions, will assess the utility of ingesting GPS TEC measurements into the model, and will endeavor to calibrate the model for high-latitude regions.

### Acknowledgments

Infrastructure funding for CHAIN was provided by the Canada Foundation for Innovation and the New Brunswick Innovation Foundation. CHAIN operations are conducted in collaboration with the Canadian Space Agency. Science funding is provided by the Natural Sciences and Engineering Research Council of Canada. Ionosonde data are available from the CHAIN website at <http://chain.physics.unb.ca/chain/>. Incoherent Scatter Radar data are available from the SRI International Database at <http://amisr.com/database/> or from the Madrigal Database at <http://isr.sri.com/madrigal/>. Digisonde data and ionospheric characteristics were retrieved using the Lowell DIDbase (<http://spase.info/SMWG/Observatory/GIRO>, <http://spase.info/VWO/NumericalData/GIRO/CHARS.PT15M>). The authors would like to thank the administrators of the GIRO network and Lowell DIDbase, as well as the ionosonde operators, for their continued effort to make the Qaanaaq digisonde data available.

Alan Rodger thanks the reviewers for their assistance in evaluating the paper.

### References

- Adeniyi, J. O., S. M. Radicella, I. A. Adimula, A. A. Willoughby, O. A. Oladipo, and O. Olawepo (2008), Validation of B0 and B1 in the IRI 2001 model at low solar activity for Ilorin an equatorial station, *Adv. Space Res.*, *42*, 691–694, doi:10.1016/j.asr.2007.09.42.
- Altadill, D., J. M. Torta, and E. Blanch (2009), Proposal of new models of the bottomside B0 and B1 parameters for IRI, *Adv. Space Res.*, *42*, 610–616, doi:10.1016/j.asr.2008.08.0144.
- Bahcivan, H., R. T. Tsunoda, M. J. Nicolls, and C. J. Heinselman (2010), Initial ionospheric observations made by the new Resolute incoherent scatter radar and comparison to solar wind IMF, *Geophys. Res. Lett.*, *37*, L15103, doi:10.1029/2010GL043632.
- Belehaki, A., and I. Tsagouri (2002), Investigation of the relative bottomside/topside contribution to the total electron content estimates, *Ann. Geophys.*, *45*(1), 73–86.
- Bilitza, D. (1990), International Reference Ionosphere 1990, NSSDC 90-22, Greenbelt, Md.
- Bilitza, D. (2001), International Reference Ionosphere 2000, *Radio Sci.*, *36*(2), 261–275, doi:10.1029/2000RS002432.
- Bilitza, D. (2003), International Reference Ionosphere 2000: Examples of improvements and new features, *Adv. Space Res.*, *31*(3), 757–767.
- Bilitza, D. (2004), A correction for the IRI topside electron density model based on Alouette/ISIS topside sounder data, *Adv. Space Res.*, *33*, 838–843, doi:10.1016/j.asr.2003.07.009.
- Bilitza, D. (2009), Evaluation of the IRI-2007 model options for the topside electron density, *Adv. Space Res.*, *44*, 701–706, doi:10.1016/j.asr.2009.04.036.
- Bilitza, D., and B. W. Reinisch (2008), International Reference Ionosphere 2007: Improvements and new parameters, *Adv. Space Res.*, *42*, 599–609, doi:10.1016/j.asr.2007.07.048.
- Bilitza, D., N. M. Sheikh, and R. Eyfrig (1979), A global model for the height of the F2-peak using M3000 values from the CCIR numerical map, *Telecommun. J.*, *46*, 549–553.
- Bilitza, D., S. M. Radicella, B. W. Reinisch, J. O. Adeniyi, M. E. Mosert Gonzalez, and S. R. Zhang (2000), New B0 and B1 models for IRI, *Adv. Space Res.*, *25*(1), 89–95.
- Bilitza, D., L.-A. McKinnell, B. W. Reinisch, and T. Fuller-Rowell (2010), The international reference ionosphere today and in the future, *J. Geodes.*, *85*, 909–920, doi:10.1007/s00190-010-0427-x.
- Bilitza, D., S. A. Brown, M. Y. Wang, J. R. Souza, and P. A. Roddy (2012), Measurements and IRI model predictions during the recent solar minimum, *J. Atmos. Sol. Terr. Phys.*, *86*, 99–106, doi:10.1016/j.jastp.2012.06.010.
- Blanch, E., D. Arrazola, D. Altadill, D. Buresova, and M. Mosert (2007), Improvement of IRI B0, B1 and D1 at mid-latitude using MARP, *Adv. Space Res.*, *39*, 701–710, doi:10.1016/j.asr.2006.08.007.
- Bust, G. S., J. W. Garner, and T. L. Gaussiran (2004), Ionospheric data assimilation three-dimensional (IDA3D): A global multisensor, electron density specification algorithm, *J. Geophys. Res.*, *109*, A11312, doi:10.1029/2003JA010234.
- Coisson, P., S. M. Radicella, and B. Nava (2002), Comparisons of experimental topside electron concentration profiles with IRI and NeQuick models, *Ann. Geophys.*, *45*(1), 111–116.
- Coisson, P., S. M. Radicella, R. Leitinger, and B. Nava (2006), Topside electron density in IRI and NeQuick: Features and limitations, *Adv. Space Res.*, *37*, 937–942.
- Coisson, P., B. Nava, and S. M. Radicella (2009), On the use of NeQuick topside option in IRI-2007, *Adv. Space Res.*, *43*, 1688–1693, doi:10.1016/j.asr.2008.10.035.
- Ehinlafa, O. E., O. A. Falaiye, and J. O. Adeniyi (2010), Comparison of observed hmF<sub>2</sub> and IRI 2007 model with M(3000)F<sub>2</sub> estimation of hmF<sub>2</sub> at low solar activity for an equatorial station, *Adv. Space Res.*, *46*, 89–93, doi:10.1016/j.asr.2010.02.018.
- Evans, J. (1969), Theory and practice of ionosphere study by Thomson scatter radar, *Proc. IEEE*, *57*(4), 496–530.
- Ezquer, R. G., M. A. Cabrera, J. L. Lopez, M. R. Albornoz, M. Mosert, P. Marco, and D. Buresova (2011), Critical frequency and maximum electron density of F2 region over four stations in the North American sector, *J. Atmos. Sol. Terr. Phys.*, *73*, 420–429, doi:10.1016/j.jastp.2010.09.018.
- Galkin, I. A., B. W. Reinisch, X. Huang, and D. Bilitza (2012), Assimilation of GIRO data into a real-time IRI, *Radio Sci.*, *47*, R50L07, doi:10.1029/2011RS004952.
- Gulyaeva, T. L. (1987), Progress in ionospheric informatics based on electron density profile analysis of ionograms, *Adv. Space Res.*, *7*(6), 39–48.
- Gulyaeva, T. L. (2003), International standard model of the Earth's ionosphere and plasmasphere, *Astron. Astrophys. Trans.*, *22*(4), 639–643.
- Hernandez-Pajares, M., J. Juan, J. Sanz, and D. Bilitza (2002), Combining GPS measurements and IRI model values for space weather specification, *Adv. Space Res.*, *29*(6), 949–958.
- Jayachandran, P. T., et al. (2009), Canadian High Arctic Ionospheric Network (CHAIN), *Radio Sci.*, *44*, R50A03, doi:10.1029/2008RS004046.
- Jodalen, V., T. Bergsvik, P. S. Canon, and P. C. Arthur (2001), Performance of HF modems on high-latitude paths using multiple frequencies, *Radio Sci.*, *36*, 1687–1698, doi:10.1029/2000RS002547.
- Komjathy, A., R. B. Langley, and D. Bilitza (1998), Ingesting GPS-derived TEC data into the international reference ionosphere delay corrections, *Adv. Space Res.*, *22*(6), 793–801.
- Lee, C. C., and B. W. Reinisch (2012), Variations in equatorial F2-layer parameters and comparison with IRI-2007 during a deep solar minimum, *J. Atmos. Sol. Terr. Phys.*, *74*, 217–223, doi:10.1016/j.jastp.2011.11.002.
- Lühr, H., and C. Xiong (2010), IRI-2007 model overestimates electron density during the 23/24 solar minimum, *Geophys. Res. Lett.*, *37*, L23101, doi:10.1029/2010GL045430.
- MacDougall, J., and P. T. Jayachandran (2007), Polar patches: Auroral zone precipitation effects, *J. Geophys. Res.*, *112*, A05312, doi:10.1029/2006JA011930.

- Magdaleno, S., D. Altadill, M. Herraiz, E. Blanch, and B. de la Morena (2011), Ionospheric peak height behavior for low, middle, and high latitudes: A potential empirical model for quiet conditions – Comparison with IRI-2007 model, *J. Atmos. Sol. Terr. Phys.*, *73*, 1810–1817, doi:10.1016/j.jastp.2011.04.019.
- Maltseva, O. A., N. S. Mozhaeva, and T. V. Nikitenko (2013), Comparison of model and experimental ionospheric parameters at high latitudes, *Adv. Space Res.*, *51*(4), 599–609, doi:10.1016/j.asr.2012.04.009.
- McKinnell, L.-A., O. Chimidza, and P. Cilliers (2009), The variability and predictability of the IRI B0, B1 parameters over Grahamstown, South Africa, *Adv. Space Res.*, *44*, 747–755, doi:10.1016/j.asr.2009.05.019.
- Moskaleva, E. V., and N. Y. Zaalov (2013), Signature of polar cap inhomogeneities in vertical sounding data, *Radio Sci.*, *48*, 547–563, doi:10.1002/rds.20060.
- Oyeyemi, E. O., A. O. Adewale, A. B. Adeloye, and A. O. Akala (2010), Comparison between IRI-2001 predictions and observed measurements of hmF<sub>2</sub> over three high latitude stations during different solar activity periods, *J. Atmos. Sol. Terr. Phys.*, *72*, 676–684, doi:10.1016/j.jastp.2010.03.009.
- Pezzopane, M., M. Pietrella, A. Pignatelli, B. Zolesi, and L. R. Cander (2011), Assimilation of autoscaled data and regional and local ionospheric models as input sources for real-time 3-D International Reference Ionosphere modeling, *Radio Sci.*, *46*, RS5009, doi:10.1029/2011RS004697.
- Reinisch, B. W., I. A. Galkin, G. Khmyrov, A. Kozlov, and D. F. Kitrosser (2004), Automated collection and dissemination of ionospheric data from the digisonde network, *Adv. Radio Sci.*, *2*, 241–247.
- Reinisch, B. W., X. Huang, I. A. Galkin, V. Paznukhov, and A. Kozlov (2005), Recent advances in real-time analysis of ionograms and ionospheric drift measurements with Digisondes, *J. Atmos. Sol. Terr. Phys.*, *67*, 1054–1062.
- Schmidt, M., D. Bilitza, C. Shum, and C. Zeilhofer (2008), Regional 4D modeling of the ionospheric electron density, *Adv. Space Res.*, *42*(4), 782–790, doi:10.1016/j.asr.2007.02.050.
- Sethi, N. K., and K. K. Mahajan (2002), The bottomside parameters B0, B1 obtained from incoherent scatter measurements during a solar maximum and their comparisons with the IRI-2001 model, *Ann. Geophys.*, *20*, 817–822.
- Sethi, N. K., and V. K. Pandey (2001), Comparative study of electron density from incoherent scatter measurements at Arecibo with the IRI-95 model during solar maximum, *Ann. Geophys.*, *18*, 1630–1634.
- Sethi, N. K., R. S. Dabas, and K. Sharma (2008), Comparison between IRI predictions and digital ionosonde measurements of hmF<sub>2</sub> at New Delhi during low and moderate solar activity, *J. Atmos. Sol. Terr. Phys.*, *70*, 756–763, doi:10.1016/j.jastp.2007.10.009.
- Smith, N. (1939), The relation of radio sky-wave transmission to ionosphere measurements, *Proceedings of the I.R.E.* (May), pp. 332–347.
- Themens, D. R., P. T. Jayachandran, R. B. Langley, J. W. MacDougall, and M. J. Nicolls (2013), Determining receiver biases in GPS-derived total electron content in the auroral oval and polar cap region using ionosonde measurements, *GPS Solutions*, *17*(3), 357–369, doi:10.1007/s10291-012-0284-6.
- Titheridge, J. E. (1985), Ionogram analysis: Least-squares fitting of a Chapman layer peak, *Radio Sci.*, *20*(2), 247–256, doi:10.1029/RS020i002p00247.
- Titheridge, J. E. (1988), The real height analysis of ionograms: A generalized formulation, *Radio Sci.*, *23*(5), 831–849, doi:10.1029/RS023i005p00831.
- Wichaipanich, N., P. Supnithi, T. Tsugawa, T. Maruyama, and T. Nagatsuma (2012), Comparison of ionosphere characteristic parameters obtained by ionosonde with IRI-2007 model over Southeast Asia, *Adv. Space Res.*, *52*(10), 1748–1755, doi:10.1016/j.asr.2012.06.018.
- Wieder, B. (1955), Some results of a sweep-frequency propagation experiment over an 1150 km east–west path, *J. Geophys. Res.*, *60*(4), 395–409, doi:10.1029/JZ060i004p00395.